11th International Symposium on Turbulence and Shear Flow Phenomena (TSFP11)
Southampton, UK, July 30 to August 2, 2019

# DIRECT NUMERICAL SIMULATION OF TURBULENT FLOW IN A SUDDEN-CONTRACTED CHANNEL

**Xingjun Fang**
Department of Mechanical Engineering
University of Manitoba
Winnipeg, MB, R3T 5V6, Canada
fangx@myumanitoba.ca

**Mark F. Tachie**
Department of Mechanical Engineering
University of Manitoba
Winnipeg, MB, R3T 5V6, Canada
mark.tachie@umanitoba.ca

**Donald J. Bergstrom**
Department of Mechanical Engineering
University of Saskatchewan
Saskatoon, Saskatchewan, S7N 5A9, Canada
don.bergstrom@usask.ca

## ABSTRACT

In this paper, direct numerical simulation is conducted to investigate the spatio-temporal characteristics of turbulent separation induced by a forward-facing step (FFS) with an oncoming fully-developed channel flow. The alteration mechanism of separation bubbles by the oncoming vortical structures is also studied in terms of the evolution of an idealized hairpin structure in the mean turbulent flow. The results indicate that the two separation bubbles upstream and over the FFS are quasi-periodic in both time and the spanwise direction. With an enlarged separation bubble upstream the FFS, the separation bubble over the FFS is shrunk and can break into two recirculation bubbles. This is attributed to the induction mechanism of hairpin vortices leaning over the FFS. As a hairpin structure approaches the FFS, the two legs, a pair of counter-rotating vortices, are stretched and consequently pump the flow backward to enlarge the separation bubble in front of the FFS. Meanwhile, a pair of opposite counter-rotating streamwise vortices are induced in the near-wall region over the FFS, and therefore generate a strong sweep event over the FFS to reduce and breakup the separation bubble.

## INTRODUCTION

Separating and reattaching turbulent flows are of pivotal importance to the transport and mixing in fluid machinery. An in-depth understanding about the flow physics of separating and reattaching turbulent flows is routinely sought from turbulent flows impinging onto a forward-facing step (FFS).

The flow characteristics of fully-developed laminar channel flow over an FFS have been studied experimentally and numerically. By employing the hydrogen bubble technique and particle tracking velocimetry, Stüer *et al.* (1999) investigated the separation bubble in front of an FFS submerged in a fully-developed laminar channel flow for Reynolds numbers, which are defined based on the half channel height and mean velocity, between 270 and 2400. They observed that the fluid entrained into the separation bubble is released over the step in streaks that are quasi-periodic in the spanwise direction. Wilhelm *et al.* (2003) performed linear stability analysis and direct numerical simulation (DNS) of the fully-developed laminar channel flow over an FFS. They concluded that, at Reynolds number 330, the flow over the FFS was stable, and demonstrated that the three-dimensional streamline pattern in front of the FFS observed by Stüer *et al.* (1999) was due to a 'wavenumber selection process' in response to the unavoidable white noise in the experimental environment. Lanzerstorfer & Kuhlmann (2012) studied the effect of different step heights on the linear instability of the full-developed laminar channel flow over an FFS. They observed that the critical Reynolds number decreases monotonically as the step height increases. Regardless of the step height, the critical mode possesses the strongest production near the rear part of the separating streamline due to streamwise counter-rotating vortices. It is also worth noting here that Stüer *et al.* (1999), Wilhelm *et al.* (2003) and Lanzerstorfer & Kuhlmann (2012) all observed the existence of streamwise counter-rotating vortices over the FFS with a spanwise periodicity of approximately three step height.

Over the past decades, turbulent flows over an FFS have been extensively investigated, and abundant knowledge has been accumulated on the effects of Reynolds number, wall roughness condition, and step height on the flow statistics (Hattori & Nagano, 2010; Essel & Tachie, 2017). Recent investigations on this topic have focused on the interactions of oncoming turbulence structures with separation bubbles (Pearson *et al.*, 2013; Fang & Tachie, 2019). Pearson *et al.* (2013) and Fang & Tachie (2019) used planar time-resolved particle image velocimetry to study the separation bubble in front of an FFS, and the separation bubbles over and behind a forward-backward-facing step (FBFS), respectively. Both studies attributed the low-frequency flapping motion of the separation bubble in front of the FFS and that over the FBFS to the streamwise elongated streaky structures embedded in theoncoming turbulent boundary layer (TBL). Moreover, Fang & Tachie (2019) observed that the separation bubble over the FBFS breaks up into dual recirculation regions at a frequency

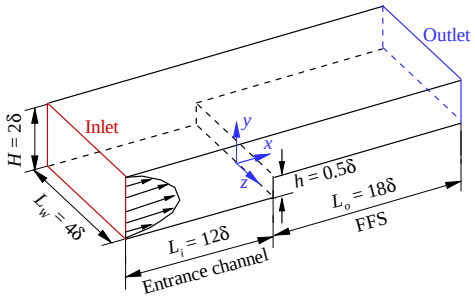


Figure 1. Schematic of computation domain (not to scale) and the coordinate system.

higher than the flapping motion, which was attributed to the instability of the separation bubble triggered by the streamwise vortical structures over the step. These observations by Pearson *et al.* (2013) and Fang & Tachie (2019) reflect some important imprints of the interactions of hairpin packets (Adrian *et al.*, 2000) residing in a TBL with FFS or FBFS. Since a planar PIV system was used in these experimental investigations, the complete three velocity components in all three dimensions were not available, and as a consequence, the three-dimensionality of the separation bubble and impinging vortical structures was not comprehensively analyzed. Therefore, this research aims at investigating the unsteady three-dimensional characteristics of turbulent separations induced by FFS, with particular attention to the interaction of oncoming hairpin vortices and the separation bubbles.

## TEST CASE AND NUMERICAL ALGORITHM

In this research, three types of DNS were performed: (i) turbulent flow in a sudden-contracted channel (hereafter denoted as $\mathrm{DNS_t}$); (ii) fully-developed turbulent channel flow (hereafter denoted as $\mathrm{DNS_i}$); and (iii) a single hairpin structure in the mean turbulent field of $\mathrm{DNS_t}$ (hereinafter denoted as $\mathrm{DNS_h}$).

Figure 1 shows the adopted coordinate system and the computational domain for $\mathrm{DNS_t}$. The test geometry consists of an entrance channel of height $H$ and length $L_i$ followed by an FFS of height $h$ and length $L_o$. This geometry has been used to investigate the laminar/turbulent channel flow over an FFS (Stüer *et al.*, 1999; Wilhelm *et al.*, 2003; Lanzerstorfer & Kuhlmann, 2012; Essel & Tachie, 2017). The blockage ratio ($h/H$) is fixed at 25%, i.e., $h = 0.25H$. A zero-velocity boundary condition is applied on the top and bottom walls (including the surfaces of the FFS). A periodic boundary condition is used in the spanwise ($z$) direction and a convective boundary condition is implemented at the outlet. Grid points were more clustered to the leading edge of FFS in both the $x$ and $y$ directions. 240 uniformly distributed grids were used in the $z$ direction. Overall, approximately 27.3 million independent grid points were used in the present $\mathrm{DNS_t}$.

The unsteady velocity field at the inlet plane is provided by simultaneously running $\mathrm{DNS_i}$ for a fully-developed turbulent channel flow at $Re_\tau = u_\tau\delta/\nu = 180$, where $\delta$, $u_\tau$ and $\nu$ represent the half channel height, friction velocity and kinematic viscosity, respectively. $\mathrm{DNS}_i$ uses the same computational domain (as well as grids) as the entrance channel in figure 1, which is $12\delta \times 2\delta \times 4\delta$ in the streamwise, vertical and spanwise directions, respectively. This computational domain is very close to $4\pi\delta \times 2\delta \times \frac{4}{3}\pi\delta$ that was been used in the database generated by Moser *et al.* (1999).

The continuity and Navier-Stokes (NS) equations for an incompressible flow can be expressed as

$$\frac{\partial u_i}{\partial x_i} = 0 \quad , \tag{1}$$

$$\frac{\partial u_i}{\partial t} + u_j\frac{\partial u_i}{\partial x_j} = -\frac{1}{\rho}\frac{\partial p}{\partial x_i} + \nu\frac{\partial^2 u_i}{\partial x_j^2} + f_i \quad , \tag{2}$$

respectively. In the above equations, $t$, $\rho$ and $p$ are time, density and pressure, respectively. $x_i$ with $i = 1$, 2 and 3 represent the streamwise, vertical and spanwise coordinates, respectively, which are also denoted as $x$, $y$ and $z$ for convenience. $u_i$ and $f_i$ are the velocity and body force (such as streamwise pressure gradient) in the $x_i$ direction, respectively. For conciseness in the discussion, we also use $u$, $v$ and $w$ to represent $u_1$, $u_2$ and $u_3$, respectively.

The spectral-element method (SEM) code (named as "Semtex") publicly shared by Blackburn & Sherwin (2004) under the GNU general public license (GPL) is modified exclusively for the current DNS study. This SEM code uses the object-oriented C++ language to organize the data structure, and performs highly optimized/vectorized calculation using FORTRAN language. All variables are expressed in the functional space spanned by Fourier series in the $z$ direction and Gauss-Lobatto-Legendre (GLL) Lagrange interpolants in the $x$-$y$ plane. The high-order time splitting method (Karniadakis *et al.*, 1991) is employed for time integration. Specifically, the convection and body force terms, pressure term and viscous term in equation (2) are integrated in three consecutive substeps within one time step.

In addition to investigating flow over an FFS with an oncoming fully-developed turbulent channel flow ($\mathrm{DNS}_t$), we study the dynamics of an idealized hairpin vortex in the oncoming turbulent flow. To introduce a single hairpin structure in the entrance channel, the linear stochastic estimation (LSE) technique based on the condition of an ejection event at selected reference points is used to extract the essential footprint of hairpin structures. Subsequently, the evolution of the LSE fluctuating velocity field in the background of the mean turbulent flows is traced by solving the NS equations. The numerical procedure described above was proposed by Zhou *et al.* (1999) for a turbulent channel flow, and was subsequently adopted by Kim *et al.* (2008) and Goudar *et al.* (2016). It should be noted that without the correct level of fluctuating velocities to generate the correct levels of Reynolds stresses, the mean turbulent flow cannot sustain itself under the dynamic system prescribed by the NS equations for $\mathrm{DNS_t}$. Thus, in the implementation of $\mathrm{DNS_h}$, we include the Reynolds stress gradient term in the NS equation, i.e. $f_i = -\partial\overline{u_i'u_j'}/\partial x_j$ in equation (2), where $\overline{u_i'u_j'}$ is the Reynold stress tensor acquired from $\mathrm{DNS_t}$. As such, in $\mathrm{DNS_h}$, the mean turbulent flow remains invariant without any perturbation, and the evolution of a single hairpin structure can be studied unambiguously. It should be remarked that the Reynolds stress gradient term was not implemented in the simulations performed by Zhou *et al.* (1999), Kim *et al.* (2008) and Goudar *et al.* (2016), and therefore, they did not consider the effect of decaying Reynolds number on the evolution of hairpin structures.

In this paper, operator $\overline{(\cdot)}$ denotes averaging in both time and the homogeneous spanwise ($z$) direction whenever applicable, and superscript $(\cdot)'$ denotes the fluctuating component. As such, the instantaneous streamwise velocity can be decomposed as $u = \overline{u} + u'$.

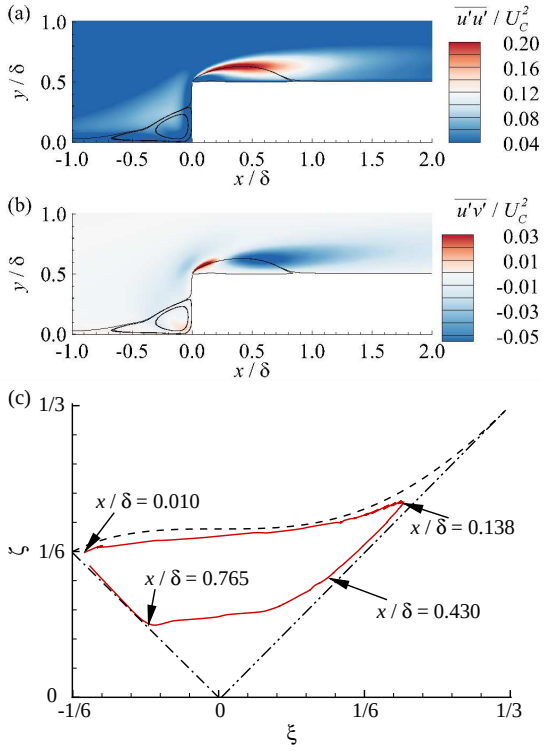


Figure 2. Contours of Reynolds stresses (a) $\overline{u'u'}$ and (b) $\overline{u'v'}$ superimposed with mean streamlines. (c) Trajectory of the invariants $\zeta = (\frac{1}{6}b_{ij}b_{ji})^{1/2}$ and $\xi = (\frac{1}{6}b_{ij}b_{jk}b_{ki})^{1/3}$ of the Reynolds stress anisotropy tensor ($b_{ij} = \overline{u_i'u_j'}/\overline{u_k'u_k'} - \frac{1}{3}\delta_{ij}$) along the separating streamline over the step. The dashed, dash-dotted and dash-dot-dotted lines represent the special states defined by $\zeta = (\frac{1}{27} + 2\xi^3)^{1/2}$, $\zeta = -\xi$ and $\zeta = \xi$, respectively, which form the boundaries of the Lumley triangle (Lumley, 1978).

## RESULTS AND DISCUSSION

As seen in figure 2, two distinct mean separation bubbles occur upstream and over the step, and are hereafter denoted by TSBF and TSBT, respectively, for conciseness. The stagnation point on the windward face of the FFS is at $y/\delta = 0.30$, i.e. $y/h = 0.60$. This compares well with $y/h = 0.59$-$0.61$ observed by Hattori & Nagano (2010) for a DNS study of a TBL over FFS with different step heights ($h/\delta \in [1/3,\ 2/3]$) at a similar Reynolds number (their Reynolds number $U_\infty h/\nu$ was 1800, as opposed to the present Reynolds number $U_C h/\nu$ 1650, where $U_C$ is themean streamwise velocity at the center of the inlet). From the separating streamline shown in figure 2, flow reattachment over the step occurs at $x = 0.86\delta$, which corresponds to a reattachment length of $1.72h$. This value is slightly smaller than that ($1.82$-$1.86h$) observed by Hattori & Nagano (2010), but larger than $1.6h$ reported by Fang & Tachie (2019) for the separation bubble over an FBFS with much stronger oncoming turbulent intensity (their root-mean-square of upstream streamwise fluctuating velocity at the body height is $u'_{rms}|_{y=h}/U_\infty = 11\%$, as oppose to $u'_{rms}|_{y=h}/U_C = 7\%$ in the present study).

The maximum Reynolds stresses occur along the separating streamline over the step. This is at variance with the observations for flows over bluff bodies immersed in laminar flows, where Reynolds stresses peak in the rear part of the separation bubble (Lanzerstorfer & Kuhlmann, 2012; Kiya & Sasaki, 1983). This difference reflects the effect of the oncoming turbulent flow. It is also evident that an area of strong positively valued $\overline{u'v'}$ occurs near the leading edge, similar to the observation of Hattori & Nagano (2010), Essel & Tachie (2017) and Fang & Tachie (2019) for turbulent flows over FFS/FBFS. By analyzing the Reynolds stresses in the curvilinear coordinate system along the streamline, Fang & Tachie (2019) concluded that the positively valued Reynolds shear stress near the leading edge is an artefact of misalignment of the streamline with the predefined streamwise direction.

As seen in figure 2(c), the topology of the Reynolds-stress ellipsoid exhibits a strong variation along the separating streamline over the FFS. Specifically, it is similar to two-component axisymmetric turbulence very close to the leading edge. In the region slightly downstream of the leading edge ($x/\delta \in [0.01,\ 0.0138]$) and along the separating streamline, it is close to a state of two-component turbulence due to very weak $\overline{v'v'}$ compared to $\overline{u'u'}$ and $\overline{w'w'}$ in this region (not shown here). As for the region of $x/\delta \in [0.0138,\ 0.430]$ in the front half of the separating streamline, the Reynolds stresses are similar to an axisymmetric state with one large eigenvalue owing to the very strong $\overline{u'u'}$ in the vicinity of the separating streamline. Downstream of the mid-point of the separation bubble ($x/\delta > 0.43$), the Reynolds stresses becomes axisymmetric with one small eigenvalue, owing to the damping effect of the wall to vertical fluctuation ($\overline{v'v'}$).

Figure 3 characterizes the reverse flow and vortical structures in a typical instantaneous flow field near the FFS. Generally speaking, the reverse flows occur in irregular shaped volumes in front of and over the FFS. In front of the FFS, the volume of reverse flow can extend across the entire height of the FFS. Stüer *et al.* (1999), Wilhelm *et al.* (2003) and Pearson *et al.* (2013) also observed that the separation bubble in front of the FFS can spill over a step with either laminar or turbulent upstream flows. As seen in the figure, the extremely high elevation of reverse flows occurs quasi-periodically in the spanwise direction. It is also interesting to note in figure 3(a) that over the FFS, reverse flow disappears in patches (marked using arrows) of a quasi-periodical nature in the spanwise direction. Straightforwardly, the $x$-$y$ planes across those intermediate reattachment patches would exhibit dual separation bubbles over the FFS, which is reminiscent of the breakup event of separation bubble over an FBFS observed by Fang & Tachie (2019). From figure 3(b), the density of vortical structures suddenly increases as the FFS approached, and the vortical structures leaning over the FFS are preferentially aligned in the streamwise-vertical planes. Downstream of the leading edge of the FFS, spanwise orientated vortical structures begin to appear, and eventually a 'forest' of hairpins appear. By comparing figures 3(a) and (b), the vortical structures leaning over the FFS coincide with the large volumes of reverse flow in front of the FFS.

To further understand the spanwise length scales of the reverse flow, the areas of reverse flow in the $x$-$y$ plane at different spanwise locations were calculated for both TSBF and TSBT, which are denoted by $A_F$ and $A_T$, respectively. Figure 4(a) shows the premultiplied spectra of $A_F$ and $A_T$ in terms of spanwise wavelength ($\lambda_z$). From the figure, $A_F$ possesses a dominant spanwise periodicity of 119 wall units. On the other hand, the dominant spanwise periodicity of $A_T$ is $1.34\delta$, corresponding to $2.68h$. This is reminiscent of the spanwise periodicity of approximately three step heights observed by Stüer *et al.* (1999), Wilhelm *et al.*

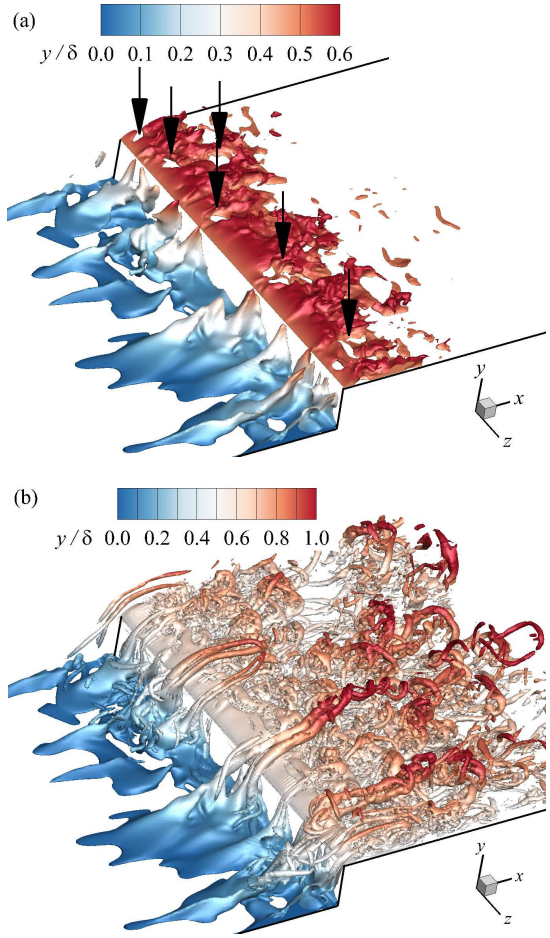


Figure 3. (a) Isosurface of the reverse flow ($u < 0$) near the forward-facing step. The thick arrows mark intermediate reattachment regions leading to dual separation bubbles in the $x$-$y$ plane. (b) Superposition of the isosurfaces of reverse flow and $\lambda_{ci}\delta/U_C = 5$. The isosurfaces are colored with the vertical coordinate ($y$).

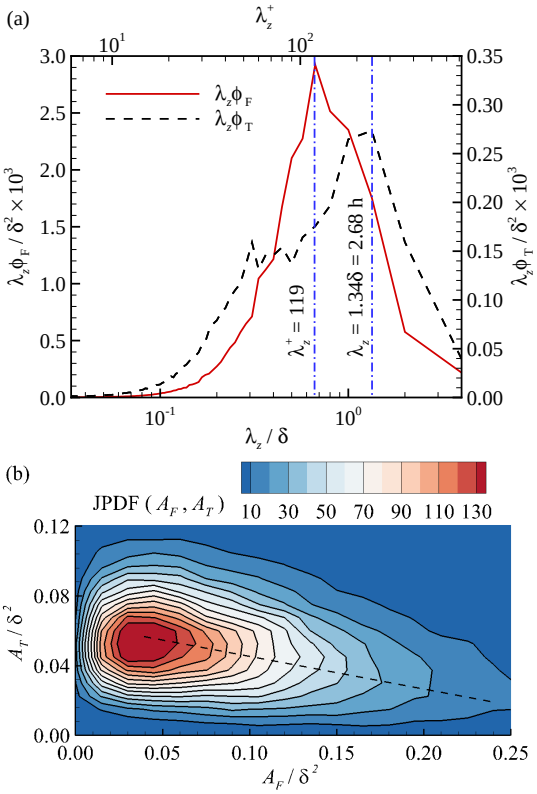


Figure 4. (a) Premultiplied spectra of reverse flow areas in front of ($A_F$) and over ($A_T$) the FFS. (b) Joint probability density function (JPDF) of $A_F$ and $A_T$. The dashed line estimates the inclination of the farthest points of isopleths.

(2003) and Lanzerstorfer & Kuhlmann (2012) for flows over an FFS. From figure 4(b), the horizontal extent of the isopleths are typically larger than the corresponding vertical extents. This indicates that the variation range of $A_F$ is larger than that of $A_T$. In addition, the isopleths shown in figure 4(b) are clearly inclined downwards (see the dashed line), and reflects an interesting deduction that a large separation bubble in front of the FFS is associated with a small separation bubble over the step.

To investigate the unsteadiness of TSBF and TSBT, figure 5 shows the temporal cross-correlation ($R_{FT}(\Delta t)$) and premultiplied frequency spectra ($\phi_{FF}$ and $\phi_{TT}$) of $A'_F$ and $A'_T$. From the figure, the value of $R_{FT}(\Delta t)$ possesses a distinct negative peak centered at $\Delta t U_C/h = 2.9$. This suggests that an expansion of TSBF leads to a shrinkage of TSBT after a time delay of $2.9h/U_C$. Graziani *et al.* (2018) observed dual negative peaks in $R_{FT}(\Delta t)$ for a TBL over an FFS. As seen in figure 5(b), $f\phi_{FF}$ possesses a sharp peak at $St = fh/U_C = 0.033$, whereas $f\phi_{TT}$ exhibits dual peaks at $St = 0.082$ and $0.146$, respectively. The dual peak pattern is similar to that for the separation bubble over an FBFS observed by Fang & Tachie (2019).

Figure 6 shows the temporal evolution of a single hairpin structure. In the figure, the spanwise elongated isosurfaces indicate the vortical cores of two mean separation bubbles. The mean separation bubbles stay invariant when the planted hairpin structure is away from the step. This reflects the effectiveness of our modified numerical procedure of Zhou *et al.* (1999). As time increases, the hairpin grows in size and moves further away from the wall. Particularly, the hairpin structure at $tU_C/\delta = 6$ shows a characteristic 'kink' in the legs and a pair of 'tongues' downstream the head appear, similar to the observations of Haidari & Smith (1994) and Zhou *et al.* (1999).

Figure 7 plots the time variation of $A_F$ and $A_T$ at the spanwise center of the imposed single hairpin structure. The values of $A_F$ and $A_T$ experience a sudden increase and decrease, respectively, after $tU_C/h \approx 12$. This opposite variation of $A_F$ and $A_T$ in figure 7 indicates that the downward inclination of $JPDF(A'_F, A'_T)$ in figure 4(b) and negative cross-correlation $R_{FT}$ in figure 5(a) are the manifestation of hairpin structures interacting with the separation bubbles. It is also evident in figure 7 that the variation magnitudes of $A_F$ and $A_T$ both peak around $tU_C/h \approx 17.5$.

Figure 8 shows the vortical structure and reverse flow at $tU_C/\delta = 15$. From figure 8(a), the reverse flow is significantly enlarged in front of the FFS, whereas the reverse flow over the FFS is clearly reduced. From the streamlines shown in figure 8(a), the vortical motion in the upstream corner deviates towards the upward and downward direction and forms a pair of counter-rotating vortices to enlarge the separation bubble in the center. This is consistent with the observation by Fang & Tachie (2019) that an enlarged separation bubble in front of a step is associated with a pair of counter-rotating vortices in the vertical direction. From figure 8(b), as the hairpin vortices pass over the FFS, the legs in the form of counter-rotating vortices tend to lean over the

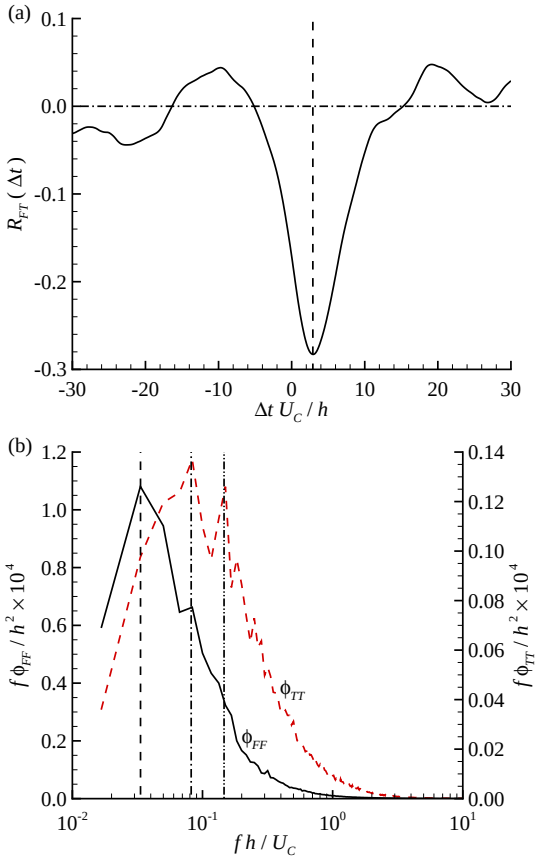


Figure 5. (a) Temporal cross-correlation ($R_{FT}(\Delta t)$) of $A'_F$ and $A'_T$. The marked vertical line is at $\Delta t U_C/h = 2.9$. (b) Premultiplied frequency spectra of $A'_F$ and $A'_T$. The marked dashed, dash-dotted and dash-dot-dotted vertical lines are at $fh/U_C = 0.033$, 0.082 and 0.146, respectively.

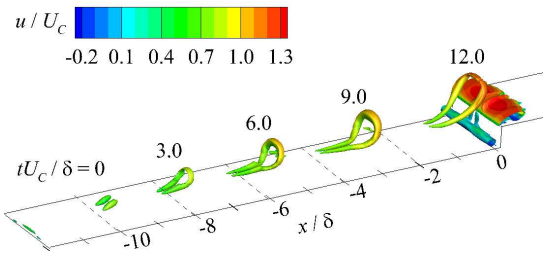


Figure 6. Time evolution of the isosurfaces of $\lambda_{ci} = U_C/\delta$ from $\mathrm{DNS_h}$.

step and stay for a long time (still visible at $tU_C/\delta = 23$). In the region downstream of TSBT over the FFS, multiple hairpin vortices appear on both sides of the oncoming hairpin vortices. In other words, one hairpin structure in the upstream location can induce multiple hairpin structures over the FFS. This provides an explanation for the observation in figure 3(b) that a forest of hairpin structures exist over the FFS, whereas only a few pairs of vortical structure lean over the leading edge. This reflects the significance of the interaction of hairpin vortex residing in turbulent flows and the FFS. For instance, it is evident from figure 8 that enlarged separation bubble in front of the FFS is induced by the legs of hairpin vortex leaning over the FFS. It is generally acknowledged that the near-wall streaky structure in turbulent flow is generated by the induction mechanism of hairpin

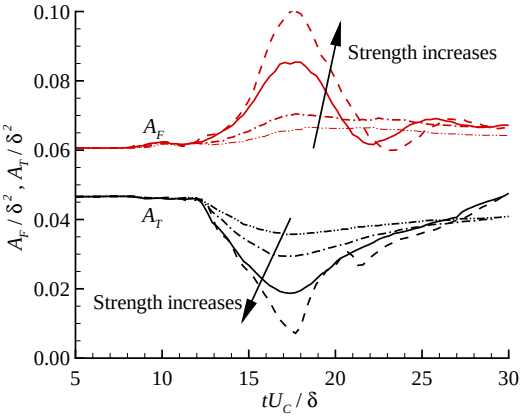


Figure 7. Time variation of $A_F$ and $A_T$ at the spanwise center of the imposed single hairpin structure. The arrow marks the variation trend as the strength of hairpin structure increases in the order of 0.5, 1.0, 2.0 and 3.0.

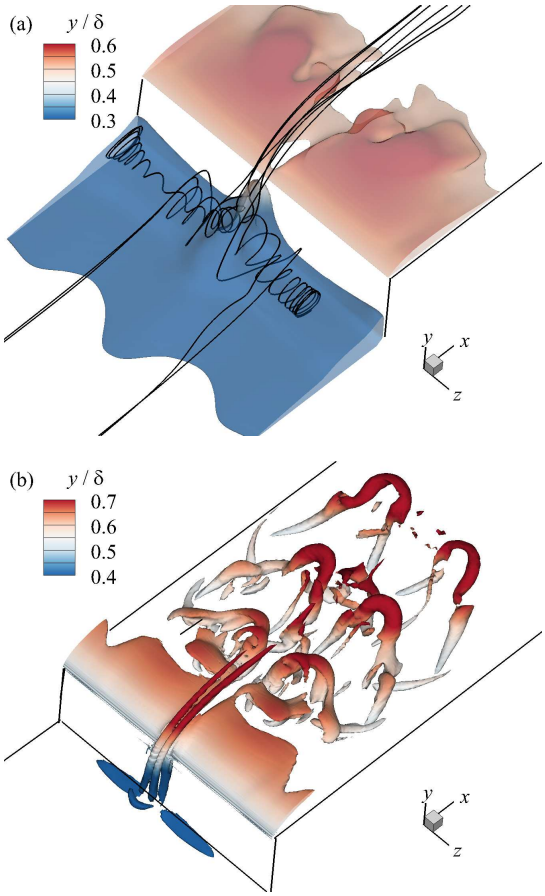


Figure 8. Isosurface of (a) reverse flow and (b) $\lambda_{ci} = 2U_C/\delta$ at $tU_C/\delta = 15$ from $\mathrm{DNS_h}$. In (a), the isosurface is made transparent to visualize the characteristic streamlines.

vortices (Adrian *et al.*, 2000). In view of these, it is expected that the dominant wavelength of $A_F$ at 119 wall units shown in figure 4(a) is close to the spanwise spacing of $\approx 100$ wall units between adjacent near-wall streaks (Jiménez & Moin, 1991).

Figure 9 further shows the flow characteristics at two selected planes in figure 8. From figure 9(a), dual separation bubble exists over the FFS. This is very similar to

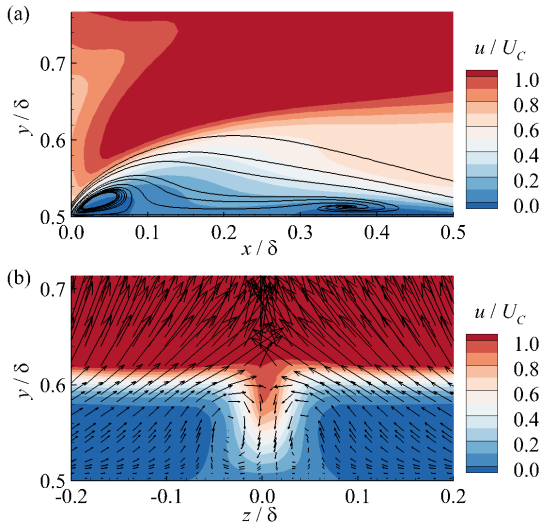


Figure 9. Contours of $u$ at $tU_C/\delta = 15$ from $\mathrm{DNS_h}$ in (a) the central $x$-$y$ plane and (b) the $z$-$y$ plane at $x/\delta = 0.2$. In-plane streamlines and velocity vectors $(w, v)$ are also plotted in (a) and (b), respectively.

the separation bubble breakup event observed by Fang & Tachie (2019) for flows over a step. As seen in figure 9(b), very close to the step surface, a pair of counter-rotating vortices with an opposite vorticity to the imposed hairpin vortices appear near the wall. Zhou *et al.* (1999) also observed similar near-wall vortices that are opposite to the primary hairpin vortices. Due to the induction of counter-rotating vortices shown in figure 9(b), high levels of streamwise momentum in the upper region are convected downwards very close to the wall, so that flow reattachment occurs to induce the dual separation bubbles over the FFS. This confirms the deduction by Fang & Tachie (2019) that the separation bubble breakup over the step is induced by the streamwise vortices associated with hairpin vortices.

## CONCLUSIONS

Turbulent flows over a forward-facing step (FFS) were studied using direct numerical simulation (DNS). Two distinct DNSs were conducted: (1) turbulent flow in a sudden contracted channel with the transient inlet boundary condition prescribed by a fully-developed turbulent channel flow (denoted by $\mathrm{DNS_t}$); and (2) a conditional eddy, which evolves into an idealized hairpin vortex, submerged in the turbulent mean flow of $\mathrm{DNS_t}$ (denoted by $\mathrm{DNS_h}$). The results were analyzed in terms of Reynolds stresses, spatio-temporal characteristics of reverse flow and vortical structures in the vicinity of the FFS.

With the incoming turbulent flow, Reynolds stresses possess peak magnitudes immediately downstream the leading edge. The topology of the Reynolds-stress ellipsoid varies significantly along the separating streamline over the FFS. In front of the FFS, localized large volumes of reverse flow occur with a spanwise periodicity of approximately 119 wall units. Over the FFS, the separation bubble possesses a spanwise periodicity of 2.67 step heights, and there exist patches of flow reattachment followed by reverse flow at a downstream location. As hairpin vortices passe over the FFS, a pair of counter-rotating vortices leaning over the leading edge persist for a long time, and an opposite pair of counter-rotating streamwise vortices over the FFS are induced in the near-wall region. Consequently, the reverse flow in front the FFS is significantly enlarged, whereas that over the FFS is diminished and broken into two distinct pieces.

## REFERENCES

Adrian, R. J., Meinhart, C. D. & Tomkins, C. D. 2000 Vortex organization in the outer region of the turbulent boundary layer. *J. Fluid Mech.* **422**, 1–54.

Blackburn, H. M. & Sherwin, S. J. 2004 Formulation of a Galerkin spectral element-Fourier method for three-dimensional incompressible flows in cylindrical geometries. *J. Comp. Phys.* **197(2)**, 759–778.

Essel, E. E. & Tachie, M. F. 2017 Upstream roughness and Reynolds number effects on turbulent flow structure over forward facing step. *Int. J. Heat Fluid Flow* **66**, 226–242.

Fang, X. & Tachie, M. F. 2019 On the unsteady characteristics of turbulent separations over a forward-backward-facing step. *J. Fluid Mech.* **863**, 994–1030.

Goudar, M. V., Breugem, W.-P. & Elsinga, G. E. 2016 Auto-generation in wall turbulence by the interaction of weak eddies. *Phys. Fluids* **28**, 035111.

Graziani, A., Kerhervé, F., Martinuzzi, R. J. & Keirsbulck, L. 2018 Dynamics of the recirculating areas of a forward-facing step. *Exper. Fluids* **59**, 154.

Haidari, A. H. & Smith, C. R. 1994 The generation and regeneration of single hairpin vortices. *J. Fluid Mech.* **277**, 135–162.

Hattori, H. & Nagano, Y. 2010 Investigation of turbulent boundary layer over forward-facing step via direct numerical simulation. *Int. J. Heat Fluid Flow* **31(3)**, 284–294.

Jiménez, J. & Moin, P. 1991 The minimal flow unit in near-wall turbulence. *J. Fluid Mech.* **225**, 213–240.

Karniadakis, G. E., Israeli, M. & Orszag, S. A. 1991 High-order splitting methods for the incompressible Navier-Stokes equations. *J. Comp. Phys.* **97(2)**, 414–443.

Kim, K., Sung, H. J. & Adrian, R. J. 2008 Effects of background noise on generating coherent packets of hairpin vortices. *Phys. Fluids* **20**, 105107.

Kiya, M. & Sasaki, K. 1983 Structure of a turbulent separation bubble. *J. Fluid Mech.* **137**, 83–113.

Lanzerstorfer, D. & Kuhlmann, H. C. 2012 Three-dimensional instability of the flow over a forward-facing step. *J. Fluid Mech.* **695**, 390–404.

Lumley, J. L. 1978 Computational modelling of turbulent flows. *Adv. Appl. Mech.* **18**, 123–176.

Moser, R. D., Kim, J. & Mansour, N. N. 1999 Direct numerical simulation of turbulent channel flow up to $Re_\tau = 590$. *Phys. Fluids* **11(4)**, 943–945.

Pearson, D. S., Goulart, P. J. & Ganapathisubramani, B. 2013 Turbulent separation upstream of a forward-facing step. *J. Fluid Mech.* **724**, 284–304.

Stüer, H., Gyr, A. & Kinzelbach, W. 1999 Laminar separation on a forward facing step. *Eur. J. Mech. B/Fluids* **18**, 675–692.

Wilhelm, D., Härtel, C. & Kleiser, L. 2003 Computational analysis of the two-dimensional-three-dimensional transition in forward-facing step flow. *J. Fluid Mech.* **489**, 1–27.

Zhou, J., Adrian, R. J., Balachandar, S. & Kendall, T. M. 1999 Mechanisms for generating coherent packets of hairpin vortices in channel flow. *J. Fluid Mech.* **387**, 353–396.